Identification of weak non-canonical base pairs around riboswitch-ligand recognition sites by solid-state NMR exchange spectroscopy

Sha Zhao
Peking University
Ziyang Wen
Peking University
Xinming Li
Tsinghua University
Mengbing zou
Peking University
Ge Yu
East China University of Science and Technology
Xiangyang Liu
East China University of Science and Technology
Lixin Zhang
East China University of Science and Technology
Yi Xue
Tsinghua University
Riqiang Fu
National High Magnetic Field Laboratory https://orcid.org/0000-0003-0075-0410
Shenlin Wang (wangshenlin@pku.edu.cn)
Peking University

Article

Keywords: RNA, solid-state NMR exchange spectroscopy

Posted Date: January 28th, 2021

DOI: https://doi.org/10.21203/rs.3.rs-152428/v1

Identification of weak non-canonical base pairs around riboswitch-ligand recognition sites by solid-state NMR exchange spectroscopy

Sha Zhao[1,2], Ziyang Wen[1], Xinming Li[3], Mengbing Zou[1,2], Ge Yu[6], Xiangyang Liu[6], Lixin Zhang[6], Yi Xue[3,*], Riqiang Fu[4,*], Shenlin Wang[1,2,5,6,7,*]

1. College of Chemistry and Molecular Engineering, Peking University, Beijing, 100871, China
2. Beijing NMR Center, Peking University, Beijing, 100871, China
3. Beijing Advanced Innovation Center for Structural Biology, Tsinghua-Peking Joint Center for Life Sciences, School of Life Sciences, Tsinghua University, Beijing 100084, China
4. National High Magnet Field lab, 1800 East Paul Dirac Drive, Tallahassee, FL, 32310, USA
5. Beijing National Laboratory for Molecular Sciences, Beijing, China
6. State Key Laboratory of Bioreactor Engineering, East China University of Science and Technology, Shanghai 200237, China
7. State Key Laboratory of Medicinal Chemical Biology, NanKai University, Tianjin 300071, China

*Corresponding author: Shenlin Wang, Yi Xue, Riqiang Fu
E-mail: wangshenlin@pku.edu.cn, yixue@mail.tsinghua.edu.cn, rfu@magnet.fsu.edu

Dedicated to the 100th anniversary of Chemistry at Nankai University.

Abstract

Base pairs are fundamental building blocks of RNA structures, and their stability and open-close equilibrium constitutes the dynamic picture. Weak base pairs, which feature the characteristics of low stability and rapid base pair opening, often play a critical role in RNA functions. However, site-specific identification of weak base pairs in RNA is challenging. Here, we report a solid-state NMR (SSNMR)-based two-dimensional proton-detected water–RNA exchange spectroscopy (WaterREXSY) to address this challenge. The approach uses the chemical exchange between hydrogen-bonded imino protons within the base pair and excited water molecules to polarize the imino protons for SSNMR observation. This process takes advantages that the imino protons within weak pairs undergo fast exchange rates with water, enabling a quick build-up and efficient detection. This method is used to characterize the weak pair in the riboA71–adenine complex (i.e., the 71nt-aptamer domain of the *add* adenine riboswitch from *Vibrio vulnificus*). We identify U47•U51, a weak non-canonical base pair that constitutes the U47•U51•(adenine-U74) base tetrad around the ligand-binding pocket. This result suggests that the breakage of U47•U51 may be the early stage in the process of ligand release.

Introduction:

Base pairs formed by inter-nucleotide hydrogen bonds are the basic building blocks of RNA structures. Each base pair involves a complex hierarchy of internal motions on various time scales.[1-4] The relative stability of an individual base pair determines the thermodynamics and kinetics of its open–close equilibrium, and this stability generally depends on the base pair type and the sequence context.[5] Stable base pairs, e.g. G–C and A–U, constitute the scaffold of the RNA structure and have slow opening rates. In contrast, weak base pairs, which are frequently non-canonical, have relatively low stability and fast opening rate.[5-7] In particular, these weak base pairs often have seminal effects on RNA folding,[8] local structural stability,[6,9] and site-specific catalysis in ribozymes.[10,11] For examples, the weak U•U base pairs are key contributors to junction stability in RNA duplexes.[6] The G•U wobble base pairs are the major structural motifs of some tRNA and rRNA.[10,11] The weak hydrogen-bonds determine the catalytic activity of ribozymes.[12,13] Identification of these weak base pairs would provide valuable insights into the dynamics and mechanisms of RNAs.

The site-specific identification of weak base pairs is challenging.[6,14,15] Solution NMR spectroscopy uses water magnetization transfer methods to measure the ^{1}H relaxation parameters mediated by water-RNA exchanges as indicators of the thermodynamics and kinetics of base pair opening equilibrium.[16,17] However, solution NMR is often limited by molecule size and is not suitable in dealing with insoluble large RNA complex[18]. In recent years, solid-state NMR (SSNMR) has emerged rapidly as an important tool in RNA studies.[19-29] This approach has unique advantages for studying RNAs across a broad range of molecular sizes,[23,24,27] and has shown great potential in studies of RNA aggregates, i.e., those involved in liquid–liquid phase separation systems.[30] In particular, the SSNMR-based hydrogen–deuterium exchange has been used to characterize RNA–protein interactions.[31] A deuterium line shape analysis provided the overall dynamics of 29-nt RNA hairpin within the messeger RNAs of HIV-1.[32] More recently, it was possible for high-resolution SSNMR spectra to be used for the study on hydrated non-crystallized RNAs in solid state, within which some local ternary structural interactions remained native.[33] However, SSNMR methods for the site-specific characterization of weak base pairs in RNA molecules

have not been established yet. Such methodology is urgently needed in this emerging field of research.

In this study, we have developed an SSNMR-based two-dimensional (2D) ^{1}H-^{15}N water–RNA exchange spectroscopy (WaterREXSY) scheme to detect weak RNA base pairs. Our approach uses the chemical exchange between the hydrogen-bonded imino protons within base pairs and water molecules to excite the imino signals. Because of their fast opening dynamics, the weak base pairs experience more frequent exchanges between iminos and water, which lead to a rapid build-up and strong cross-peaks on WaterREXSY spectra. In contrast, very stable base pairs are weakly or not detected because of their slow exchange rates. Therefore, this approach allows the efficient detection of weak base pairs in RNA.

Here, we have used this strategy to characterize the weak non-canonical base pairs in the adenine-bound form of a 71-nt aptamer domain of the *add* adenine riboswitch (riboA71). This purine riboswitch regulates *add* gene expression upon adenine binding.[34] The riboA71–adenine complex adopts a tuning fork-like fold with three stems, and the three-way helical junction where the stems meet constitutes the adenine-binding pocket. Upon adenine binding, three uridines in riboA71 and adenine form a complex hydrogen bond network, resulting in a base tetrad with adenine (Figure 1).[34-38] Using our 2D WaterREXSY approach, we demonstrated that the imino proton of U47 within the U47•U51 base pair involved in ligand binding represents a weak base pair with an imino-water exchange rate of 379 ± 57 s^{-1} at 15 °C. The U47•U51 base pair in the minor groove of the riboA71 adenine-binding pocket encompasses the complex hydrogen bond network with the U47•U51•(adenine-U74) base tetrad. The molecular dynamics simulation showed that U47•U51, but not other base pairs within the tetrad, experiences an equilibrium between the formation and breakage of the base pair. This result suggests that the open of the U47•U51 base pair may be involved in the early stage of complex dissociation upon ligand release.

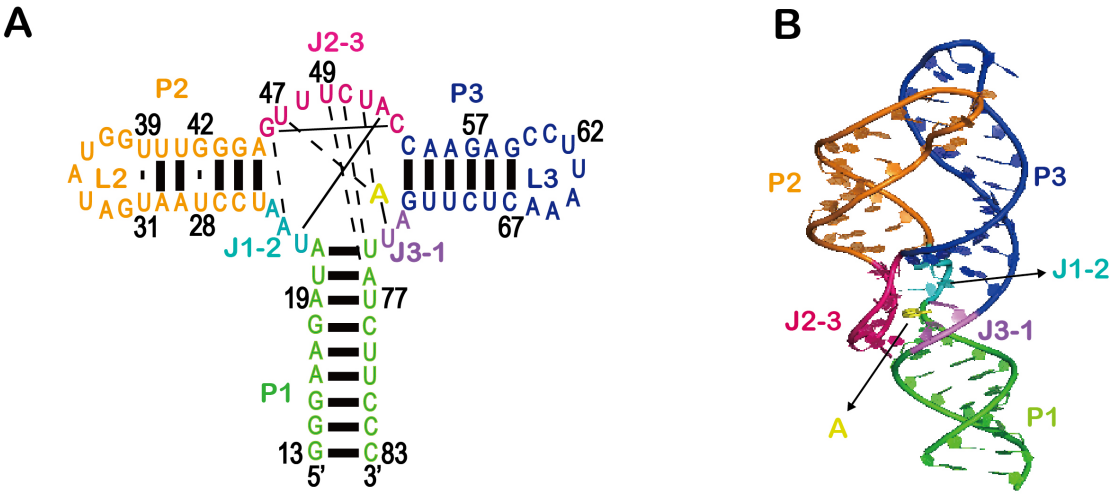

Figure 1. Secondary and crystal structure of riboA71 in the adenine-bound form. Stems P1, P2(L2) and P3(L3) are shown in green, orange and blue. Junction-connecting segments J1-2, J2-3 and J3-1 are colored cyan, hot pink and violet. The character "A" in B presents the adenine ligand. The dash lines represents the non-canonical base pairs.

Results

2D WaterREXSY experiments to identify weak base pairs in RNA

Differences in base pair stability within RNA can be determined by investigating the chemical exchange between the hydrogen-bonded imino protons and water molecules. According to the "open-close model," base pairs in RNA experience equilibrium between the open state, wherein hydrogen bonds are broken, and the closed state, wherein hydrogen bonds are formed (Supplementary Figure 2).[17,39] In the open state, imino protons are exchangeable with bulk water, and this process can be used as a "probe" to characterize the thermodynamics and kinetics of the base pair opening equilibrium (Figure 2A). A stable base pair forms strong hydrogen bonds, which lead to a relatively low proportion of the open state and a slow exchange of water and protons. In contrast, the imino protons in weak base pairs have much faster exchange rates because of the less stable hydrogen bonds and more frequent base pairs in the open state. Empirically, the canonical Watson–Crick RNA base pairs, G–C and A–U, are generally very stable and have water–RNA exchange rates of 1–10 s^{-1} and 20–100 s^{-1}, respectively.[39-42] Weaker non-canonical base pairs, such as U•U pairs, establish exchange rates over a much wider range of 100–1000 s^{-1} (Figure 2B).[43]

SSNMR spectroscopy edited by the water–RNA exchange rates could be used to identify weak base pairs. Here, we designed an SSNMR-based 2D ^{1}H-^{15}N WaterREXSY experiment to achieve this target. Figure 2C shows the 2D WaterREXSY scheme. It includes two key steps: (*i*) a ^{1}H-^{15}N rotational echo double resonance (REDOR) period that dephases the initial imino proton magnetization but not the water, and (*ii*) a Lee–Goldburg (LG) ^{1}H spin-lock along the magic angle, during which the water–RNA chemical exchange occurs and repolarizes the imino magnetization. Subsequently, the imino resonances from the water–RNA exchange are recorded in the proton-detected 2D ^{1}H-^{15}N correlation spectra. Because the LG spin-lock suppresses inter-proton spin-diffusion, the scheme avoids interference from the dipolar interaction and allows the detection of pure chemical exchange. In principle, this is the 2D version of the water–protein chemical exchange scheme developed from a previously described 1D version,[44] which allowed the identification of exchanges between specific nitrogen sites and water.

The analytical solution of the Solomon equations (Eq.1 and Supplementary Information 2.2) shows that the build-up rate of the cross-peaks on 2D WaterREXSY is determined by the exchange rate, k_{ex}, and the proton relaxation time, $T_1\rho$, at the rotating frame. Figure 2D and Supplementary Figure 4 show the simulations of the time-dependent build-up in the 2D WaterREXSY experiments against the LG spin-lock times (t_{SL}). The results indicate that as the exchange rate increases, a shorter t_{SL} is needed to achieve equilibrium. At a t_{SL} of 2 ms, the intensity of an imino proton with a chemical exchange rate of 500 s^{-1} (typical for a weak base pair) would be approximately 30-fold and 3-fold stronger than those of protons with chemical exchange rates of 10 s^{-1} and 100 s^{-1} (i.e., the stable G–C and A–U base pairs), respectively. It is also worth noting that the detection of very stable base pairs under this scheme would not be applicable even at a long $t_{SL,}$ because the relaxation loss would dramatically reduce efficiency. Therefore, the WaterREXSY scheme would obtain strong cross-peaks for weak base pairs but weak cross-peaks for stable base pairs. Furthermore, fitting a build-up curve generated by a series of experiments with different t_{SL} values would yield a quantitative exchange rate k_{ex} for the observed hydrogen-bonded imino proton in a weak base pair.

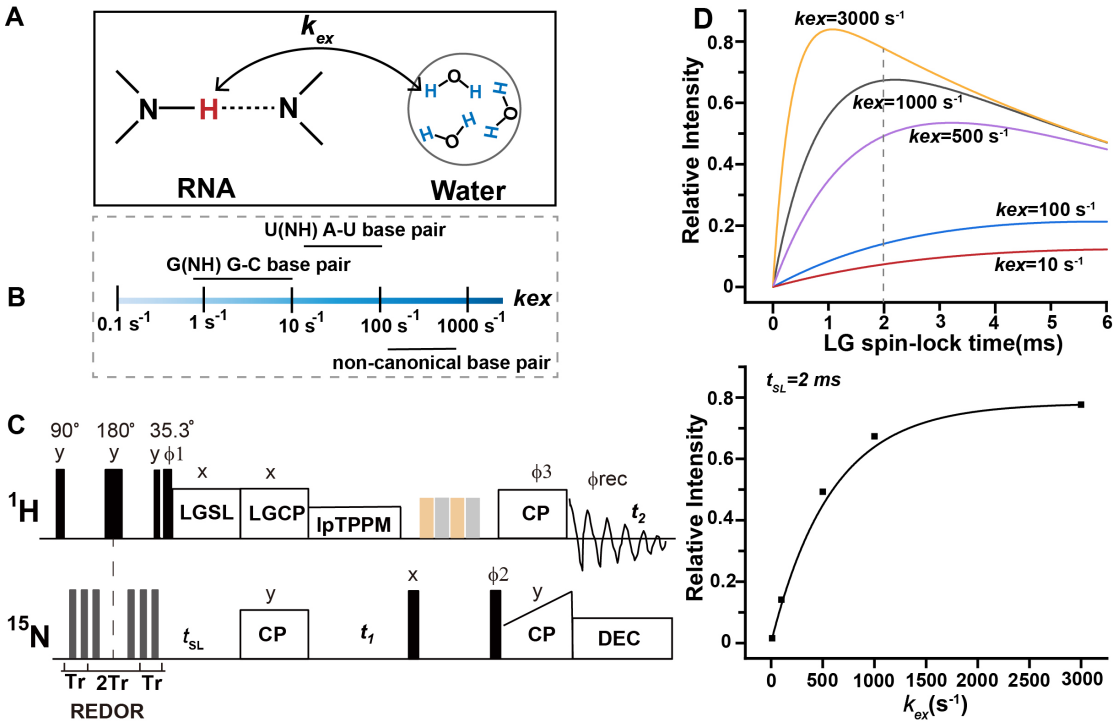

Figure 2. Theoretical considerations of the waterREXSY scheme. (A) Simplified water-RNA exchange model. The imino protons are highlighted in red, and the protons in water are highlighted in blue. k_{open} represents the base pair opening rate, k_{close} represents the reformation of hydrogen bonds and $k_{ex,\ open}$ is the rate constant for imino proton transfer in the open state. (B) Numerical simulations of the time-dependent build-up in the 2D ^{1}H-^{15}N water–RNA exchange spectroscopy (WaterREXSY) experiments with $T_1\rho$ = 8 ms and $p = 10^{-6.8}$. (C) Pulse sequence of the 2D ^{1}H-^{15}N WaterREXSY experiment used to probe the chemical exchange between RNA and water.

Involvement of U47 in weak base pairs within the riboA71–adenine complex

The 2D WaterREXSY scheme was applied to the riboA71–adenine complex to identify the weak base pairs. The 2D ^{1}H-^{15}N solid-state NMR (hNH) spectrum and several 2D WaterREXSY spectra at different t_{SL} values were collected. Figure 3A shows the 2D hNH spectrum of the riboA71–adenine complex. Here, hydrogen-bonded imino protons with characteristic chemical shifts are visible, including imino groups in the uridines in both Watson–Crick A–U base pairs (^{15}N and ^{1}H chemical shifts of 163 ppm and 13–15 ppm, respectively) and non-canonical base pairs (G•U, A•U and U•U, with ^{15}N and ^{1}H chemical shifts of 157 ppm and 10–12

ppm) and the guanines in Watson–Crick G–C base pairs (^{15}N and ^{1}H chemical shifts of 145 ppm and 11–14 ppm, respectively). The 2D WaterREXSY spectra at t_{SL} values of 1.2 ms and 2 ms include only the imino signals of uridines involved in weak non-canonical base pairs (Figure 3B, C). In contrast, the imino peaks within the canonical A–U and G–C base pairs began to appear at a t_{SL} of 3 ms (Figure 3D) or 4 ms (Figure 3E), respectively. These iminos within the A–U and G–C regions of the 2D WaterREXSY spectra may represent weak canonical base pairs in riboA71, i.e., those at the edges of stems. Furthermore, rapid build-up of the -NH_2 groups was observed, consistent with the general principle of a rapid exchange between -NH_2 and water (Supplementary Figure 7).

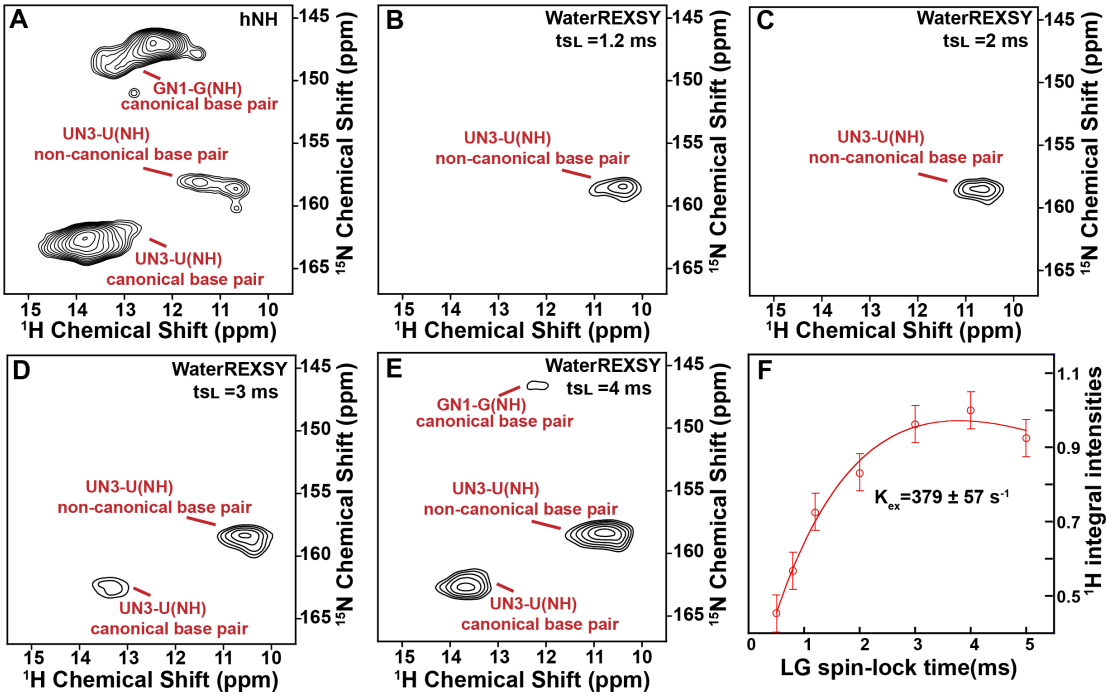

Figure 3. The WaterREXSY spectra of riboA71-adenine complex. (A) Two-dimensional (2D) hNH spectrum of the riboA71–adenine complex. (B–E) 2D water–RNA exchange spectroscopy (WaterREXSY) spectra the of riboA71–adenine complex at different spin-lock times of 1.2 ms (B), 2 ms (C), 3 ms (D) and 4 ms (E). The imino group regions are shown. (F) The intensity (I) of an imino proton of U35 at different values of t_{SL}; the red line represents the fitting curve.

The above data suggests that this scheme can be used to detect uridines involved in weak non-canonical base pairs. Solution NMR spectra revealed that the riboA71–

196 adenine complex has five cross-peaks in the region corresponding to uridines within
197 non-canonical base pairs, including U28, U31 and U39 in the P2 stem and U47 and
198 U49 in J2–3 [45,46] (Supplementary Figure 8A). To obtain the site-specific assignments,
199 we prepared two additional ^{15}N,^{13}C-uridine-labeled RNA samples, including a
200 wild-type riboA71 without adenine and a U31A/G42A mutant riboA71–adenine
201 complex. The secondary structures of these two constructs were depicted in Figure 4,
202 according to the structure of wild-type riboA71 in adenine bound form (PDB code:
203 4TZX).
204 When we analyzed the ligand-free wild-type riboA71, U47 and U49 were not
205 observed on the ^{1}H-^{15}N heteronuclear single quantum coherence (HSQC) spectrum,
206 possibly due to prominent dynamics around the binding site.[35,47] Only three imino
207 groups corresponding to U28, U31 and U39 in the stems were observed in the region
208 of uridines within non-canonical base pairs on the ^{1}H-^{15}N HSQC spectrum (Figure 4).
209 These peaks are superimposable with those of riboA71–adenine on the solution NMR
210 spectrum, suggesting that local structures were preserved. Although the 2D hNH
211 SSNMR spectrum of free riboA71 contained the cross-peaks of U28 (Figure 4D), no
212 signals were detected on the 2D WaterREXSY spectrum at a t_{SL} of 2 ms (Figure 4E),
213 indicating that the weak base pair identified here does not involve the imino of U28.
214 As U31 and U39 are not observed on the 2D hNH spectrum, we cannot conclude their
215 roles.
216 In the U31A/G42A riboA71–adenine complex, G42 and U31 were mutated to
217 adenine. Consequently, the U31•U39 and U28•G42 non-canonical base pairs were
218 changed to the A31–U39 and U28–A42 canonical base pairs, respectively, which led
219 to a shift in the corresponding cross-peaks of the uridine imino groups to the
220 characteristic region corresponding to the A–U canonical base pairs. In this scenario,
221 only two imino cross-peaks, U47 and U49, remained in the region of uridines within
222 non-canonical base pairs, and these had identical chemical shifts with respect to those
223 observed in the wild-type riboA71–adenine complex (Figure 4F). Both U47 and U49
224 were observed on the 2D hNH SSNMR spectrum (Figure 4G), whereas only one
225 imino group corresponding to uridine was observed on the 2D WaterREXSY spectra
226 at a t_{SL} of 2ms. A comparison of the ^{15}N chemical shift of this cross-peak with that in
227 the 2D hNH SSNMR spectra allowed us to assign that peak as U47 (Figure 4H), thus
228 demonstrating that U47 is involved in a weak base pair. Figure 3F shows the

cross-peak intensity of the imino group of uridine in a non-canonical base pair as a function of the t_{SL} at 15 °C. The fitting of these peak intensities against the t_{SL} in accordance with Eq. 8 in the experimental sections yields a k_{ex} value of 379 ± 57 s^{-1} for U47, which is consistent with the exchange rates of weak base pairs.

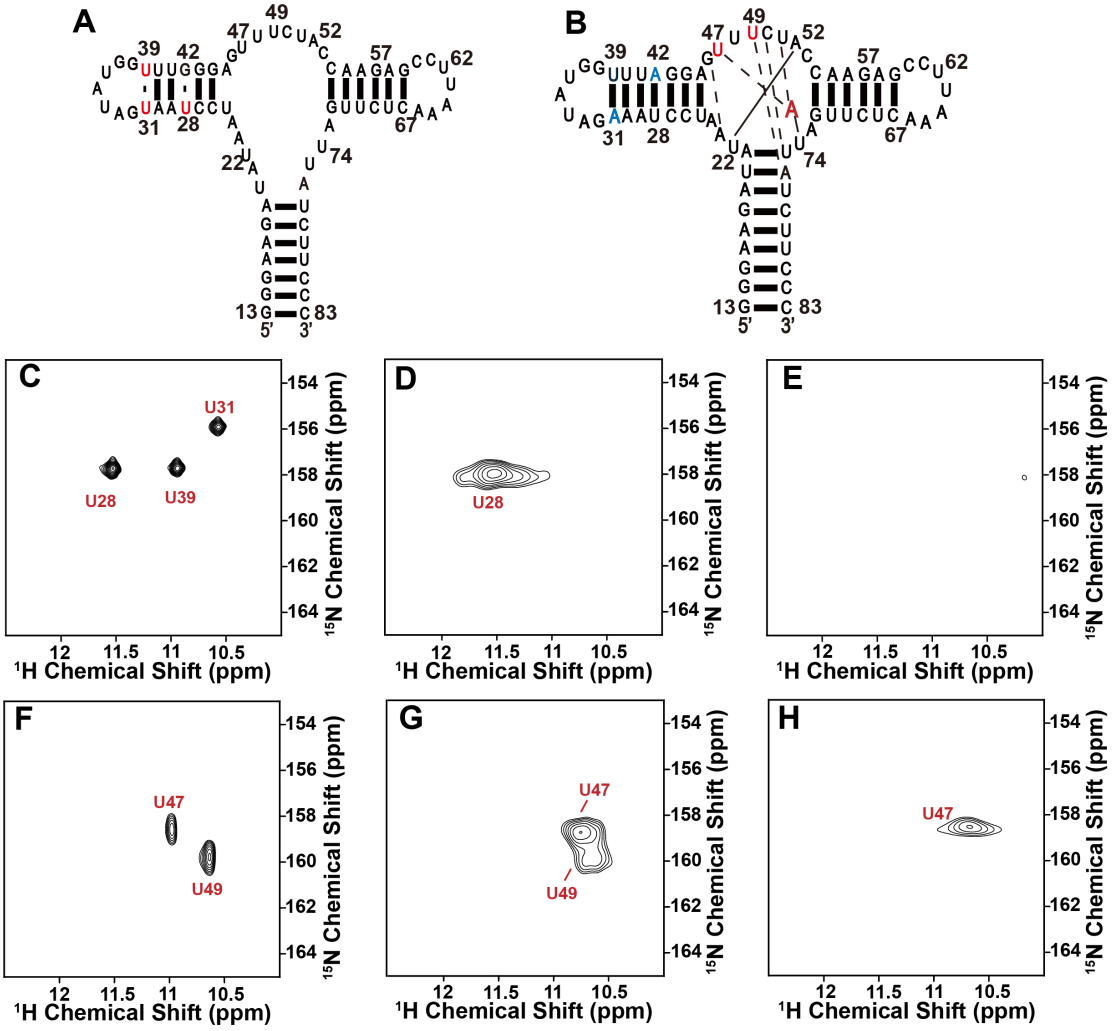

Figure 4. SSNMR and solution NMR spectra of free wild-type riboA71 and mutated riboA71-adenine complex. (A, B) Secondary structures of free wild-type riboA71 (A) and the mutated riboA71–adenine complex (B). (C) Two-dimensional (2D) ^{1}H-^{15}N HSQC spectrum of free wild-type riboA71 in solution. (D–E) 2D hNH (D) and 2D water–RNA exchange spectroscopy (WaterREXSY) spectra E) of free wild-type riboA71 in the solid state. (F) 2D ^{1}H-^{15}N HSQC spectrum of the mutated riboA71–adenine complex in solution. (G–H) 2D hNH (G) and 2D WaterREXSY spectra (H) of the mutated riboA71–adenine complex in the solid state. The spin lock-time was set at 2 ms in both 2D WaterREXSY experiments. Only the regions of uridine imino groups in non-canonical base pairs are shown.

U47 is involved in a weak base pair within the base tetrad of the ligand-binding pocket

The crystal structure of the riboA71–adenine complex has been determined (PDB: 4TZX).[34] U47 is positioned in the minor groove, where it is involved in base pairing with U51 and the bound adenine. Adenine recognition occurs through the formation of a U47•U51•(adenine-U74) base tetrad, which is centered within a five-tiered triplex structure and surrounded by other nucleotides. Two base triples, A23•(G46-C53) and A73•(A52-U22), are located above the adenine-binding site, while two other base triples, C50•(U75-A21) and U49•(A76-U20), are located below the adenine-binding site (Figure 5A). As the chemical shifts of the imino group of U47 on SSNMR spectra are almost identical to those in solution, the local structure is expected to remain in solid. Taking a close observation, only one NH···O=C hydrogen bond stabilizes the base-pair of U47•U51, whereas other non-canonical base pairs, i.e. U31•U39, U28•G42 and U49•A76 in U49•(A76-U20) base triples, have two or three inter-nucleotide hydrogen bonds, possibly forming more stable base pairs (Figure 5). Moreover, the NH···O=C is generally weaker than NH···N hydrogen bond[48], and therefore the stability of U47•U51 could be weaker than U51•adenine, although both base pairs have only one hydrogen bond.

To visualize the dynamics of the U47•U51 base pair within the U47•U51•(adenine-U74) base tetrad, we further performed a 1 μs all-atom molecular dynamics (MD) simulation, using the crystal structure (PDB: 4TZX) as the starting point. The hydrogen bonds in the U51•(adenine-U74) base triple, which are essential for the base tetrad stability, were retained throughout the simulation, indicating a very stable triple. In contrast, the open–close dynamics of the U47•U51 base pair were observed; here, the open state, wherein the hydrogen bond between U47 and U51 was broken (Figure 5B-C), had a population of approximately 4%. The hydrogen bond of U47•U51 is shown to be weaker than the other hydrogen bonds in the U51•(adenine-U74) base triple. The distances between the N3 of U47 and O4 of U51 range from 2.6 to 3.9 Å in the closed state and from 3.7 to 5.5 Å in the open state (Supplementary Materials, Movie 1). Furthermore, the imino group of U47 in the open state flips to the outside of the binding pocket, away from the

U51•(adenine-U74) base triple and more solvent-exposed, whereas in the closed state (Figure 5B), the imino proton of U47 involves a hydrogen bond with the O4 of U51 and is more solvent-protected. The probability of water molecules within 3 Å of imino proton of U47 in the open and close state was also calculated using the MD simulation. The statistical results show that the probability of the existence of water molecules around U47 in the open and close state are 95% and 12.5%, respectively, in aggrement with the observation that the solvent accessibility of U47 imino proton in the open state is ~8-fold higher than close state (Supplementary Figure 9). Thus, our MD data is consistent with the SSNMR results, in which the U47 •U51 base pair is less stable and prone to more frequently opening dynamics.

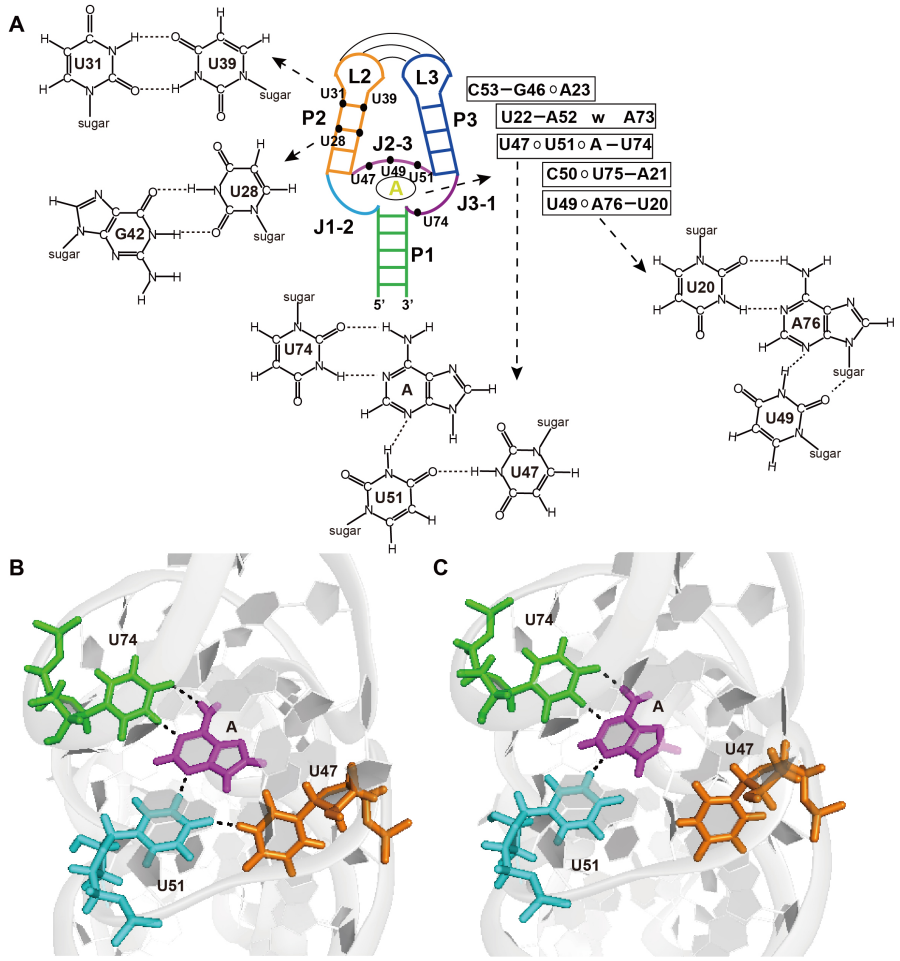

Figure 5. The topological view of riboA71-adenine complex. (A)The locations of the non-canonical base-pairs involving uridines are highlighted in the structure, e.g., U31, U39, U28 on stem P2 and U47, U49, U51 on J2-3. U31•U39, U28•G42 non-canonical base pairs are shown on the left of the model. Five-tiered arrangement of bases are shown on the right of model and (U20-A76) •U49 base triple,

U47•U51•(adenine-U74) base tetrad are also shown. (B-C) Close(B) and open(C) state of U47•U51 base pair in U47•U51•(adenine-U74) base tetrad.

Discussion

Differences in base pair stability are a critical factor in RNA dynamics. Weak base pairs with relatively fast opening dynamics are particularly important to cellular processes such as RNA folding, recognition, ligand binding and catalytic activity. Detecting these weak base pairs can provide important information about RNA functions. Here, we report an SSNMR approach in which the water–RNA chemical exchange is applied to identify the site-specific weak base pairs in RNA molecules. To the best of our knowledge, this is the first report of using SSNMR method to achieve this target. Comparing to solution NMR, the SSNMR based approach is potentially advantageous for studying insoluble RNA aggregates, such as those related to neurological diseases.[30] Moreover, SSNMR has no size limitation and will potentially help identify site-specific weak base pairs in large RNAs and RNA–protein complexes, particularly when combined with site-specific or sparse isotopic-labeling techniques.[49-55] The current approach was designed as two-dimensional proton direct detected scheme, having better sensitivity and chemical shift distribution with respect to ^{13}C or ^{15}N detected approach.

Through our WaterREXSY experiments, we identified a weak non-canonical base pair in the riboA71–adenine complex: the base pair of U47•U51 within the U47•U51•(adenine-U74) base tetrad, which is the core of ligand binding pocket. The measured water–RNA exchange rate of U47 is 379 ± 57 s^{-1} at 15 °C, which indicates a weak non-canonical base pair. Our MD simulation showed the stability of the other base pairs within the U47•U51•(adenine-U74) base tetrad. U47 and U51 are the key components in the adenine-binding pocket of riboA71, and the relatively low stability of this base pair with respect to the others in the base tetrad implies that it might have a fundamental role in the ligand recognition and dissociation process.

Previous structural studies suggested the complicated folding mechanism of the aptamer domain of *add* adenine riboswitch upon ligand binding involving many distinct folding states[56]. Without the adenine ligand, two conformations co-exist in solution, but with different secondary structures. One of the apo state is similar to

ligand binding conformation, except for the structure of the ligand binding pocket and its proximity.[37] In the presence of Mg^{2+}, the ligand free state has empty, but locally structured, binding pocket. The nucleotides involving adenine binding form canonical base pairs (i.e., U47-A52) and wobble base pairs (i.e., U48 with U75 or U74) in ligand free state.[57] After ligand binding, these hydrogen bonds will break, and form different base pairs, including the base tetrad in adenine ligand recognition, i.e., (C53–G46) •A23, (U22–A52) •A73, (U74–adenine) •U51•U47, (A21–U75) •C50 and (U20–A76) •U49, which lock P1 and J2–3 together.[57] During this process, some residues undergo large conformation changes. For example, the residue U51 can swing out from the binding pocket, which allows adenine to enter the binding pocket and forms stable interaction with adenine.[58]

Our work provides new insight to understand the progression of riboA71 folding upon ligand binding and ligand release. As the U47•U51 base pair is relatively weak with respect to other base pairs around the binding pocket, we suggest that upon ligand dissociation, breakage of the weak base pair U47•U51 might be the early stage of ligand release, and U47 and U51 can subsequently switch their interaction patterns to shift the equilibrium toward a ligand-free state. Moreover, the purine family riboswitches commonly forms several base tetrads around ligand binding pockets. The weak base pairs are also potentially present around the binding pockets, which may make seminal contribution on their mechanisms.

The strategy proposed herein will facilitate a better understanding of the dynamic and folding process of the riboswitch upon ligand binding. It will therefore play an important role in investigations of the molecular mechanisms of riboswitches that regulate gene expression. It will be also help the design of riboswitches as a novel class of molecular targets when developing antibiotics and chemical tools.

Conclusions

In summary, we developed a 2D WaterREXSY experimental strategy to detect weak non-canonical base pairs in RNA. This is the first report to describe the use of SSNMR to specifically detect weak non-canonical base pairs in RNAs. The approach takes advantage of the rapid chemical exchange between iminos within weak base pairs and water, which leads to strong detection on NMR spectroscopy. The approach

was used to study on riboA71-adenine and revealed that the imino proton of U47 in the U47•U51 base pair underwent a chemical exchange with water at an exchange rate of 379 ± 57 s^{-1} at 15 °C. Other imino protons were not observed during the 2D WaterREXSY experiment at short mixing times, thus demonstrating the unique base pair opening dynamics of U47•U51 relative to other non-canonical base pairs. The weak base pair U47•U51 is within the U47•U51•(adenine-U74) base tetrad around the ligand-binding pocket, and the observed dynamics imply a dynamic ligand dissociation process.

Methods

Sample preparation

The uniform ^{15}N,^{13}C-labeled riboA71 was produced by an *in vitro* transcription reaction as previously described.[29,59] Mutant G30A/U19A-riboA71 was prepared using a similar *in vitro* transcription protocol and double-stranded DNA templates with the sequence of 5′-TTAATACGACTCACTATAGGGAAGATATAA TCCTAATGATATGGTTTGGGAGTTTCTACCAAGAGCCTTAAACTCTTGATT ATCTTCCC-3′ and its complementary sequence. The ^{15}N,^{13}C-uridine-labeled G30A/U19A-riboA71 was obtained using ^{15}N,^{13}C-rUTP and natural abundant rATP, rGTP and rCTP. Purified riboA71 was buffer-exchanged into a deuterated buffer (75% D_2O/25% H_2O, pH 6.8) containing 10 mM KH_2PO_4, 30 mM KCl and 2 mM $MgCl_2$, and concentrated to a final concentration of 700 μM. To prepare the riboA71–adenine complex, a stock adenine solution was added to the riboA71 solution to a final concentration of 5 mM; the mixture was annealed at 95 °C for 5 minutes and incubated at 0 °C for 30 minutes.

The RNA solid-state samples for SSNMR study were prepared using the ethanol-precipitation approach, following a previously described procedure.[33] Details of the sample preparation are presented in the Supplementary Materials.

Solid-state NMR spectroscopy

All of the solid-state NMR experiments were carried out on a 600 MHz Bruker Avance III spectrometer fitted with a 1.9 mm ^{1}H-X-Y magic-angle spinning (MAS) probe. Approximately 4 mg of RNA were center-packed into a 1.9-mm SSNMR rotor.

All experiments were performed under an effective temperature of 15 °C and a MAS frequency of 40 kHz. The temperatures were calibrated using the T_1 relaxation time of ^{79}Br in KBr powder. [33] The typical π/2 pulse lengths were 2.5 μs for ^{1}H, 4.0 μs for ^{13}C and 5.0 μs for ^{15}N.

The dipolar-based 2D hNH experiments were performed using a previously reported pulse sequence.[60] The diagram of the pulse sequence (Supplementary Figure 1A) and the details of the experimental parameters are described in the Supplementary Materials.

The 2D ^{1}H-^{15}N water–RNA exchange spectroscopy (WaterREXSY) was performed using the pulse sequence described in Figure 2C. Compared to the 2D hNH experiments, the 2D WaterREXSY experiments included two additional blocks: a ^{1}H-^{15}N REDOR block and a ^{1}H LG spin-lock along the magic angle. A series of 2D WaterREXSY experiments with different spin-lock times (t_{SL}) were collected, and the 1D ^{1}H slices with a ^{15}N chemical shift of 158.6 ppm were used to create the plot of ^{1}H signals versus t_{SL}. According to Eq. 1 (below), the exchange rate could be obtained after fitting the curves of the ^{1}H signal intensities with different t_{SL} values. Details of the exchange model under the LG spin-lock as described by the Solomon equations are shown in the Supplementary Materials.

$$I(t_{SL}) = \{I(0) + A[1 - \exp(-k_{ex}\, t_{SL})]\} exp\left(-t_{SL}/T_{1\square}\right). \quad (1)$$

Molecular dynamics (MD) simulations

The initial structure used in the MD simulation was obtained from the crystal structure of riboA71-adenine complex (PDB ID: 4TZX)[61]. Hydrogen atoms were added to the adenine ligand by using Discovery Studio 3.5[62].The partial charges were calculated using the antechamber module of the Amber 18 package[63] and the AM1-BCC method. The general AMBER force-field (GAFF) parameter was used for the adenine ligand, and the other parameters required for the ligand were generated by parmchk.[64] The energy minimization and MD simulation were carried out using the GPU accelerated version of pmemd in AMBER. The nonbonded cutoff was set at 9 Å. DSSR [cite https://academic.oup.com/nar/article/43/21/e142/2468098] was used to analyze the formation of hydrogen bonds in the MD trajectory at an interval of 1 ps.

Acknowledgements

All of the solid-state NMR experiments were conducted at the Beijing NMR Center and the NMR Facility at the National Center for Protein Sciences at Peking University. The work was supported by the National Key Research and Development Program of the Ministry of Science and Technology of the People's Republic of China (contract number 2016YFA0501203), the National Natural Science Foundation of China (21874004, 91953104), the State Key Laboratory of Medicinal Chemical Biology (2020031), and the Beijing National Laboratory for Molecular Sciences. Dr. R. Fu thanks the support from the National High Magnetic Field Laboratory, which is supported by NSF Cooperative Agreement NSF/DMR-1644779 and the State of Florida. The authors thank Dr. Xiaogang Niu and Dr. Hongwei Li of Peking University for assistance in collecting solution NMR data.

Funding: Funding for this research was provided by the National Key Research and Development Program of the Ministry of Science and Technology of the People's Republic of China (2016YFA0501203), the National Natural Science Foundation of China (grant number 21874004 and 91953104), the State Key Laboratory of Medicinal Chemical Biology (2020031) and an NSF Cooperative Agreement (NSF/DMR-1644779).

Author contributions: Y.X, R.F. and S.W. designed the project. S.Z., Z.W. and M.Z. prepared the RNA samples. R.F. and S.W. developed the solid-state NMR pulse sequences. S.Z. collected the solution and the solid-state NMR spectra. X.L. and Y.X. performed the molecular dynamics simulation. S.Z. prepared the initial draft. R.F., Y.X., L.Z. Y.G., X.L., and S.W. finalized the manuscript. All of the authors edited the manuscript.

Competing interests: The authors claim no competing interests.

References:

1 Marusic, M., Schlagnitweit, J. & Petzold, K. RNA Dynamics by NMR Spectroscopy. *Chembiochem* **20**, 2685-2710, doi:10.1002/cbic.201900072 (2019).

2 Rinnenthal, J. *et al.* Mapping the landscape of RNA dynamics with NMR spectroscopy. *Acc Chem Res* **44**, 1292-1301, doi:10.1021/ar200137d (2011).

3 Nguyen, P. & Qin, P. Z. RNA dynamics: perspectives from spin labels. *Wiley Interdiscip Rev RNA* **3**, 62-72, doi:10.1002/wrna.104 (2012).

4 Al-Hashimi, H. M. & Walter, N. G. RNA dynamics: it is about time. *Curr Opin Struct Biol* **18**, 321-329, doi:10.1016/j.sbi.2008.04.004 (2008).

5 Kierzek, R., Burkard, M. E. & Turner, D. H. Thermodynamics of single mismatches in RNA duplexes. *Biochemistry* **38**, 14214-14223, doi:10.1021/bi991186l (1999).

6 Sheng, J., Gan, J., Soares, A. S., Salon, J. & Huang, Z. Structural insights of non-canonical U*U pair and Hoogsteen interaction probed with Se atom. *Nucleic Acids Res* **41**, 10476-10487, doi:10.1093/nar/gkt799 (2013).

7 Heus, H. A. & Hilbers, C. W. Structures of non-canonical tandem base pairs in RNA helices: review. *Nucleosides Nucleotides Nucleic Acids* **22**, 559-571, doi:10.1081/NCN-120021955 (2003).

8 Manosas, M., Junier, I. & Ritort, F. Force-induced misfolding in RNA. *Phys Rev E Stat Nonlin Soft Matter Phys* **78**, 061925, doi:10.1103/PhysRevE.78.061925 (2008).

9 Okada, K. *et al.* Solution structure of a GAAG tetraloop in helix 6 of SRP RNA from Pyrococcus furiosus. *Nucleosides Nucleotides Nucleic Acids* **25**, 383-395, doi:10.1080/15257770600683979 (2006).

10 Juneja, A., Villa, A. & Nilsson, L. Elucidating the Relation between Internal Motions and Dihedral Angles in an RNA Hairpin Using Molecular Dynamics. *J Chem Theory Comput* **10**, 3532-3540, doi:10.1021/ct500203m (2014).

11 Roy, A., Panigrahi, S., Bhattacharyya, M. & Bhattacharyya, D. Structure, stability, and dynamics of canonical and noncanonical base pairs: quantum chemical studies. *J Phys Chem B* **112**, 3786-3796, doi:10.1021/jp076921e (2008).

12 Krasovska, M. V., Sefcikova, J., Spackova, N., Sponer, J. & Walter, N. G. Structural dynamics of precursor and product of the RNA enzyme from the hepatitis delta virus as revealed by molecular dynamics simulations. *J Mol Biol* **351**, 731-748, doi:10.1016/j.jmb.2005.06.016 (2005).

13 Kraut, S. *et al.* Three critical hydrogen bonds determine the catalytic activity of the Diels-Alderase ribozyme. *Nucleic Acids Res* **40**, 1318-1330, doi:10.1093/nar/gkr812 (2012).

14 Wohnert, J. *et al.* Direct identification of NH...N hydrogen bonds in non-canonical base pairs of RNA by NMR spectroscopy. *Nucleic Acids Res* **27**, 3104-3110, doi:10.1093/nar/27.15.3104 (1999).

15 Masquida, B. & Westhof, E. On the wobble GoU and related pairs. *RNA* **6**, 9-15, doi:10.1017/s1355838200992082 (2000).

16 Lee, J. H. & Pardi, A. Thermodynamics and kinetics for base-pair opening in the P1 duplex of the Tetrahymena group I ribozyme. *Nucleic Acids Res* **35**, 2965-2974, doi:10.1093/nar/gkm184 (2007).

17 Szulik, M. W., Voehler, M. & Stone, M. P. NMR analysis of base-pair opening kinetics in DNA. *Curr Protoc Nucleic Acid Chem* **59**, 7 20 21-18, doi:10.1002/0471142700.nc0720s59 (2014).

18 Bothe, J. R. *et al.* Characterizing RNA dynamics at atomic resolution using solution-state NMR spectroscopy. *Nat Methods* **8**, 919-931, doi:10.1038/nmeth.1735 (2011).

19 Marchanka, A., Kreutz, C. & Carlomagno, T. Isotope labeling for studying RNA by solid-state NMR spectroscopy. *J Biomol NMR* **71**, 151-164, doi:10.1007/s10858-018-0180-7 (2018).

20 Yang, Y. & Wang, S. RNA Characterization by Solid-State NMR Spectroscopy. *Chemistry* **24**, 8698-8707, doi:10.1002/chem.201705583 (2018).

21 Carlomagno, T. Present and future of NMR for RNA-protein complexes: a perspective of integrated structural biology. *J Magn Reson* **241**, 126-136, doi:10.1016/j.jmr.2013.10.007 (2014).

22 Riedel, K. *et al.* Constraints on the structure of (CUG)97 RNA from magic-angle-spinning solid-state NMR spectroscopy. *Angew Chem Int Ed Engl* **45**, 5620-5623, doi:10.1002/anie.200600769 (2006).

23 Leppert, J. *et al.* Identification of NH...N hydrogen bonds by magic angle spinning solid state NMR in a double-stranded RNA associated with myotonic dystrophy. *Nucleic Acids Res* **32**, 1177-1183, doi:10.1093/nar/gkh288 (2004).

24 Olsen, G. L. *et al.* Monitoring tat peptide binding to TAR RNA by solid-state 31P-19F REDOR NMR. *Nucleic Acids Res* **33**, 3447-3454, doi:10.1093/nar/gki626 (2005).

25 Olsen, G. L. *et al.* Solid-state deuterium NMR studies reveal micros-ns motions in the HIV-1 transactivation response RNA recognition site. *J Am Chem Soc* **130**, 2896-2897, doi:10.1021/ja0778803 (2008).

26 Huang, W., Varani, G. & Drobny, G. P. 13C/15N-19F intermolecular REDOR NMR study of the interaction of TAR RNA with Tat peptides. *J Am Chem Soc* **132**, 17643-17645, doi:10.1021/ja1051439 (2010).

27 Marchanka, A., Simon, B., Althoff-Ospelt, G. & Carlomagno, T. RNA structure determination by solid-state NMR spectroscopy. *Nat Commun* **6**, 7024, doi:10.1038/ncomms8024 (2015).

28 Marchanka, A., Simon, B. & Carlomagno, T. A suite of solid-state NMR experiments for RNA intranucleotide resonance assignment in a 21 kDa protein-RNA complex. *Angew Chem Int Ed Engl* **52**, 9996-10001, doi:10.1002/anie.201304779 (2013).

29 Yang, Y. *et al.* Proton-detected solid-state NMR detects the inter-nucleotide correlations and architecture of dimeric RNA in microcrystals. *Chem Commun (Camb)* **53**, 12886-12889, doi:10.1039/c7cc07483b (2017).

30 Jain, A. & Vale, R. D. RNA phase transitions in repeat expansion disorders. *Nature* **546**, 243-247, doi:10.1038/nature22386 (2017).

31 Asami, S., Rakwalska-Bange, M., Carlomagno, T. & Reif, B. Protein-RNA interfaces probed by 1H-detected MAS solid-state NMR spectroscopy. *Angew Chem Int Ed Engl* **52**, 2345-2349, doi:10.1002/anie.201208024 (2013).

32 Emani, P. S., Olsen, G. L., Echodu, D. C., Varani, G. & Drobny, G. P. Slow exchange model of nonrigid rotational motion in RNA for combined solid-state and solution NMR studies. *J Phys Chem B* **114**, 15991-16002, doi:10.1021/jp107193z (2010).

33 Zhao, S. *et al.* High-resolution solid-state NMR spectroscopy of hydrated non-crystallized RNA. *Chem Commun (Camb)* **55**, 13991-13994, doi:10.1039/c9cc06552k (2019).

34 Serganov, A. *et al.* Structural basis for discriminative regulation of gene expression by adenine- and guanine-sensing mRNAs. *Chem Biol* **11**, 1729-1741, doi:10.1016/j.chembiol.2004.11.018 (2004).

35 Gilbert, S. D., Stoddard, C. D., Wise, S. J. & Batey, R. T. Thermodynamic and kinetic characterization of ligand binding to the purine riboswitch aptamer domain. *J Mol Biol* **359**, 754-768, doi:10.1016/j.jmb.2006.04.003 (2006).

36 Batey, R. T., Gilbert, S. D. & Montange, R. K. Structure of a natural guanine-responsive riboswitch complexed with the metabolite hypoxanthine. *Nature* **432**, 411-415, doi:10.1038/nature03037 (2004).

37 Reining, A. *et al.* Three-state mechanism couples ligand and temperature sensing in riboswitches. *Nature* **499**, 355-359, doi:10.1038/nature12378 (2013).

38 Warhaut, S. *et al.* Ligand-modulated folding of the full-length adenine riboswitch probed by NMR and single-molecule FRET spectroscopy. *Nucleic Acids Res* **45**, 5512-5522, doi:10.1093/nar/gkx110 (2017).

39 Snoussi, K. & Leroy, J. L. Imino proton exchange and base-pair kinetics in RNA duplexes. *Biochemistry* **40**, 8898-8904, doi:10.1021/bi010385d (2001).

40 Mirau, P. A. & Kearns, D. R. Effect of environment, conformation, sequence and base substituents on the imino proton exchange rates in guanine and inosine-containing DNA, RNA, and DNA-RNA duplexes. *J Mol Biol* **177**, 207-227, doi:10.1016/0022-2836(84)90453-4 (1984).

41 Lee, J. H., Jucker, F. & Pardi, A. Imino proton exchange rates imply an induced-fit binding mechanism for the VEGF165-targeting aptamer, Macugen. *FEBS Lett* **582**, 1835-1839, doi:10.1016/j.febslet.2008.05.003 (2008).

42 Maltseva, T. V., Zarytova, V. F. & Chattopadhyaya, J. Base-pair exchange kinetics of the imino and amino protons of the 3'-phenazinium tethered DNA-RNA duplex, r(5'GAUUGAA3'):d(5'TCAATC3'-Pzn), and their comparison with those of B-DNA duplex. *J Biochem Biophys Methods* **30**, 163-177, doi:10.1016/0165-022x(94)00075-o (1995).

578 43 Snoussi, K., Bulte, J. W., Gueron, M. & van Zijl, P. C. Sensitive CEST agents
579 based on nucleic acid imino proton exchange: detection of poly(rU) and of a
580 dendrimer-poly(rU) model for nucleic acid delivery and pharmacology. *Magn*
581 *Reson Med* **49**, 998-1005, doi:10.1002/mrm.10463 (2003).
582 44 Fu, R., Miao, Y., Qin, H. & Cross, T. A. Probing Hydronium Ion Histidine
583 NH Exchange Rate Constants in the M2 Channel via Indirect Observation of
584 Dipolar-Dephased (15)N Signals in Magic-Angle-Spinning NMR. *J Am Chem*
585 *Soc* **138**, 15801-15804, doi:10.1021/jacs.6b08376 (2016).
586 45 Ding, J., Swain, M., Yu, P., Stagno, J. R. & Wang, Y. X. Conformational
587 flexibility of adenine riboswitch aptamer in apo and bound states using NMR
588 and an X-ray free electron laser. *J Biomol NMR* **73**, 509-518,
589 doi:10.1007/s10858-019-00278-w (2019).
590 46 Noeske, J., Schwalbe, H. & Wohnert, J. Metal-ion binding and metal-ion
591 induced folding of the adenine-sensing riboswitch aptamer domain. *Nucleic*
592 *Acids Res* **35**, 5262-5273, doi:10.1093/nar/gkm565 (2007).
593 47 Batey, R. T. Structure and mechanism of purine-binding riboswitches. *Q Rev*
594 *Biophys* **45**, 345-381, doi:10.1017/S0033583512000078 (2012).
595 48 Desiraju, G. S., T. The Weak Hydrogen Bond (2010).
596 49 Longhini, A. P. *et al.* Chemo-enzymatic synthesis of site-specific isotopically
597 labeled nucleotides for use in NMR resonance assignment, dynamics and
598 structural characterizations. *Nucleic Acids Research* **44**, doi:ARTN e52
599 10.1093/nar/gkv1333 (2016).
600 50 LeBlanc, R. M., Longhini, A. P., Le Grice, S. F. J., Johnson, B. A. & Dayie, T.
601 K. Combining asymmetric 13C-labeling and isotopic filter/edit NOESY: a
602 novel strategy for rapid and logical RNA resonance assignment. *Nucleic Acids*
603 *Res* **45**, e146, doi:10.1093/nar/gkx591 (2017).
604 51 Strebitzer, E., Nussbaumer, F., Kremser, J., Tollinger, M. & Kreutz, C.
605 Studying sparsely populated conformational states in RNA combining
606 chemical synthesis and solution NMR spectroscopy. *Methods* **148**, 39-47,
607 doi:10.1016/j.ymeth.2018.05.007 (2018).
608 52 Juen, M. A. *et al.* Excited States of Nucleic Acids Probed by Proton
609 Relaxation Dispersion NMR Spectroscopy. *Angew Chem Int Ed Engl* **55**,
610 12008-12012, doi:10.1002/anie.201605870 (2016).

53 Liu, Y. *et al.* Synthesis and applications of RNAs with position-selective labelling and mosaic composition. *Nature* **522**, 368-372, doi:10.1038/nature14352 (2015).

54 Liu, Y., Sousa, R. & Wang, Y. X. Specific labeling: An effective tool to explore the RNA world. *Bioessays* **38**, 192-200, doi:10.1002/bies.201500119 (2016).

55 Liu, Y. *et al.* Applications of PLOR in labeling large RNAs at specific sites. *Methods* **103**, 4-10, doi:10.1016/j.ymeth.2016.03.014 (2016).

56 Neupane, K., Yu, H., Foster, D. A., Wang, F. & Woodside, M. T. Single-molecule force spectroscopy of the add adenine riboswitch relates folding to regulatory mechanism. *Nucleic Acids Res* **39**, 7677-7687, doi:10.1093/nar/gkr305 (2011).

57 Stagno, J. R. *et al.* Structures of riboswitch RNA reaction states by mix-and-inject XFEL serial crystallography. *Nature* **541**, 242-246, doi:10.1038/nature20599 (2017).

58 Bao, L., Wang, J. & Xiao, Y. Molecular dynamics simulation of the binding process of ligands to the add adenine riboswitch aptamer. *Phys Rev E* **100**, 022412, doi:10.1103/PhysRevE.100.022412 (2019).

59 Milligan, J. F., Groebe, D. R., Witherell, G. W. & Uhlenbeck, O. C. Oligoribonucleotide synthesis using T7 RNA polymerase and synthetic DNA templates. *Nucleic Acids Res* **15**, 8783-8798, doi:10.1093/nar/15.21.8783 (1987).

60 Zhou, D. H. & Rienstra, C. M. High-performance solvent suppression for proton detected solid-state NMR. *J Magn Reson* **192**, 167-172, doi:10.1016/j.jmr.2008.01.012 (2008).

61 Zhang, J. & Ferre-D'Amare, A. R. Dramatic improvement of crystals of large RNAs by cation replacement and dehydration. *Structure* **22**, 1363-1371, doi:10.1016/j.str.2014.07.011 (2014).

62 BIOVIA, D. S. Discovery Studio, 3.5. *San Diego: Dassault Systèmes* (2012).

63 Case., D. A. *et al.* AMBER 2018. *University of California, San Francisco* (2018).

64 Wang, J., Wolf, R. M., Caldwell, J. W., Kollman, P. A. & Case, D. A. Development and testing of a general amber force field. *J Comput Chem* **25**, 1157-1174, doi:10.1002/jcc.20035 (2004).

647

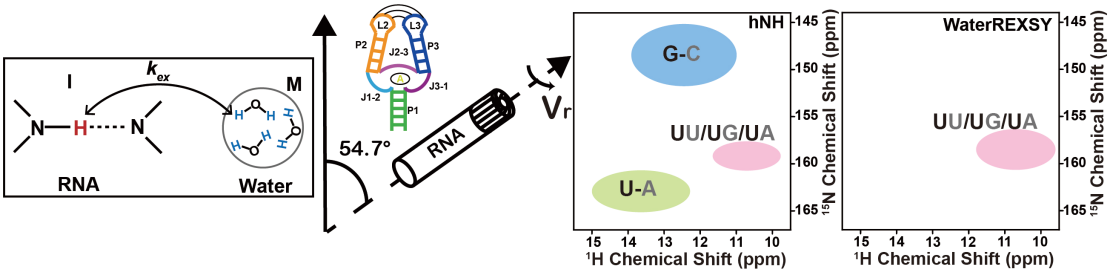

648

649 TOC: Identification of weak non-canonical base pairs around riboswitch-ligand

650 recognition sites by solid-state NMR exchange spectroscopy

651

Figures

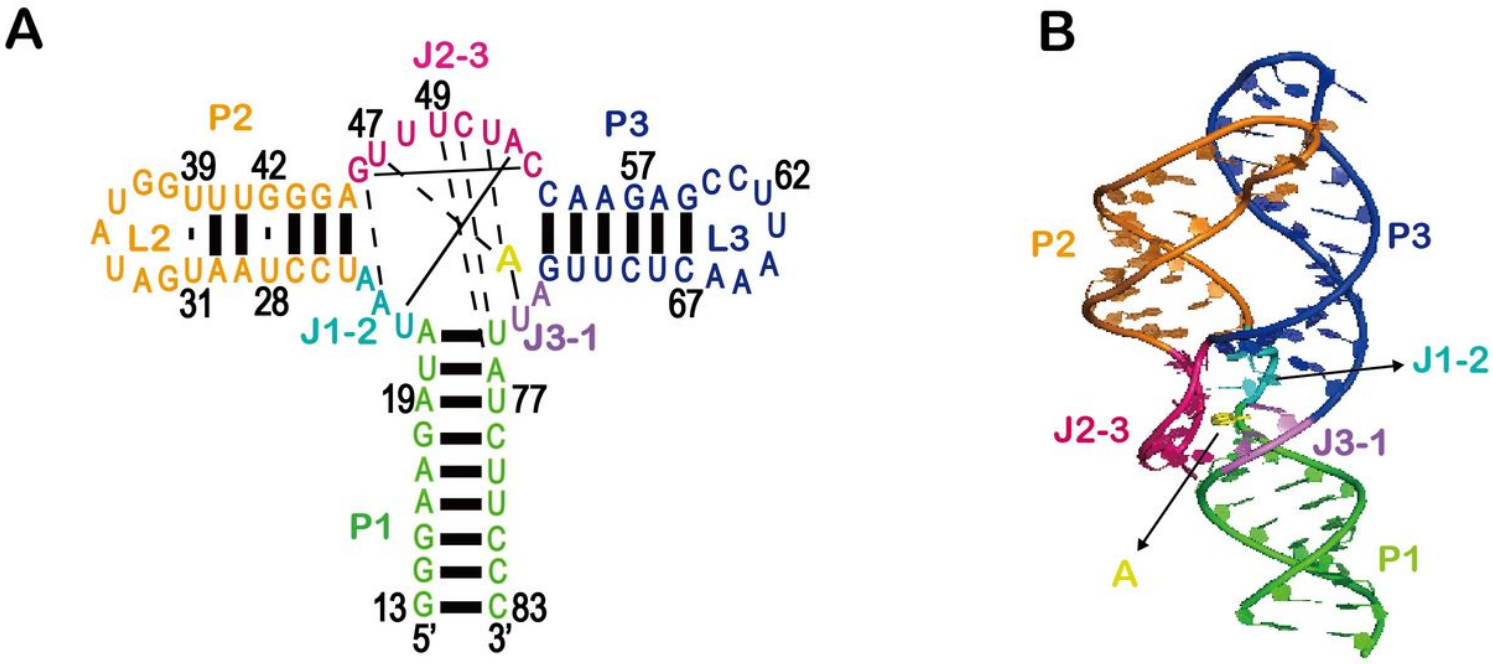

Figure 1

Secondary and crystal structure of riboA71 in the adenine-bound form. Stems P1, P2(L2) and P3(L3) are shown in green, orange and blue. Junction-connecting segments J1-2, J2-3 and J3-1 are colored cyan, hot pink and violet. The character “A” in B presents the adenine ligand. The dash lines represents the non-canonical base pairs.

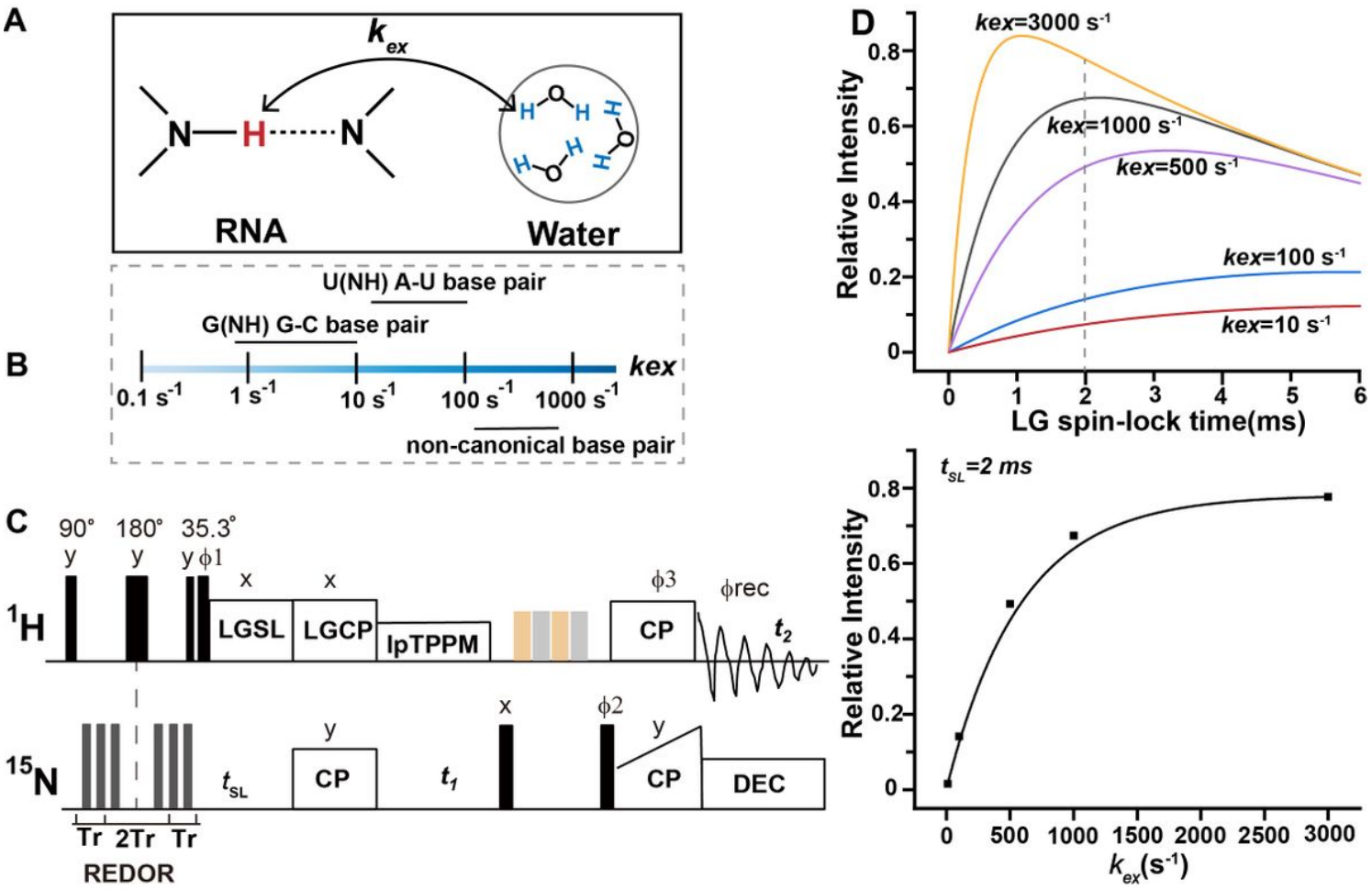

Figure 2

Theoretical considerations of the waterREXSY scheme. (A) Simplified water-RNA exchange model. The imino protons are highlighted in red, and the protons in water are highlighted in blue. kopen represents the base pair opening rate, kclose represents the reformation of hydrogen bonds and kex, open is the rate constant for imino proton transfer in the open state. (B) Numerical simulations of the time-dependent build-up in the 2D 1H-15N water–RNA exchange spectroscopy (WaterREXSY) experiments with T1ρ = 8 ms and p = 10-6.8. (C) Pulse sequence of the 2D 1H-15N WaterREXSY experiment used to probe the chemical exchange between RNA and water.

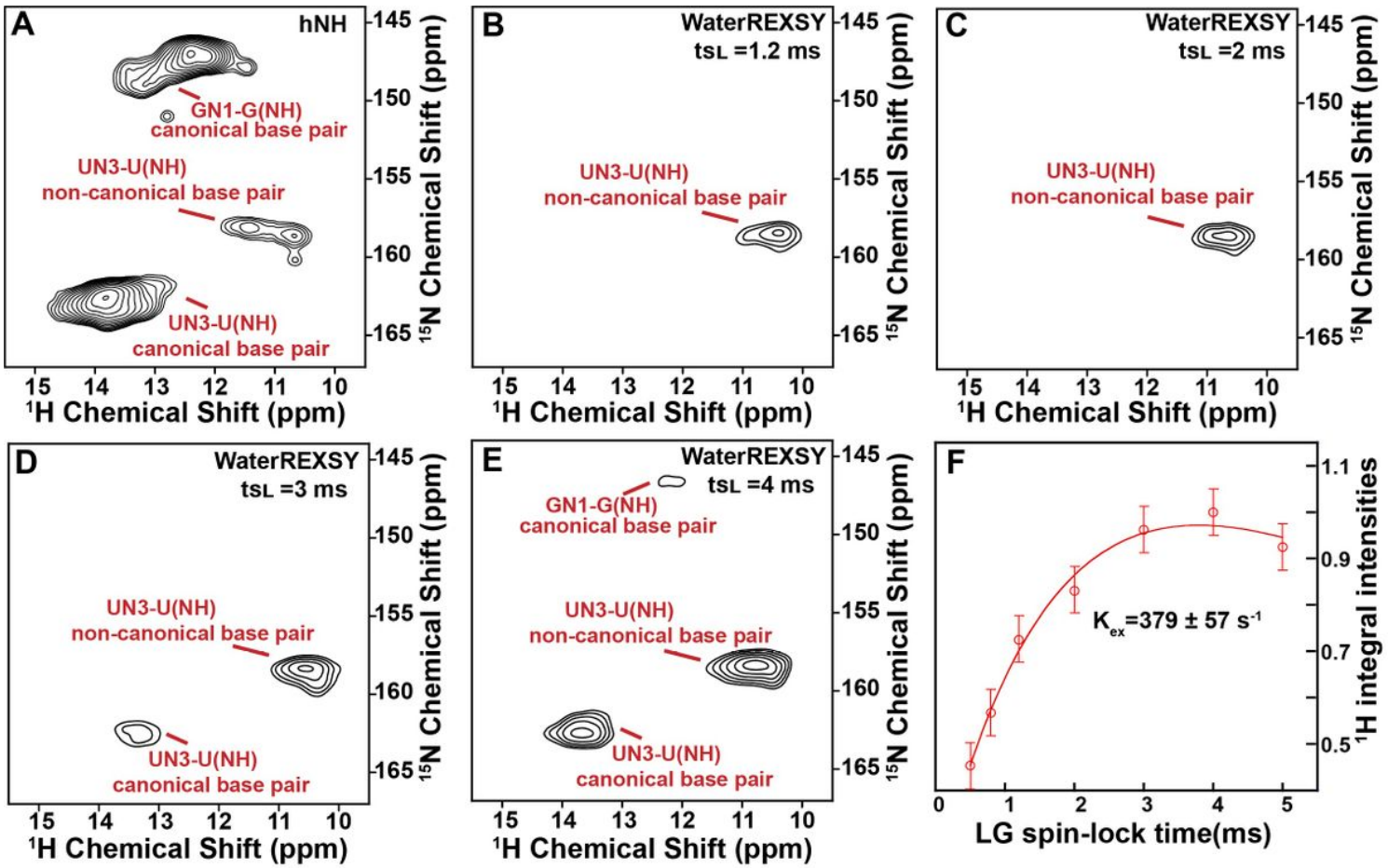

Figure 3

The WaterREXSY spectra of riboA71-adenine complex. (A) Two-dimensional (2D) hNH spectrum of the riboA71–adenine complex. (B–E) 2D water–RNA exchange spectroscopy (WaterREXSY) spectra the of riboA71–adenine complex at different spin-lock times of 1.2 ms (B), 2 ms (C), 3 ms (D) and 4 ms (E). The imino group regions are shown. (F) The intensity (I) of an imino proton of U35 at different values of tSL; the red line represents the fitting curve.

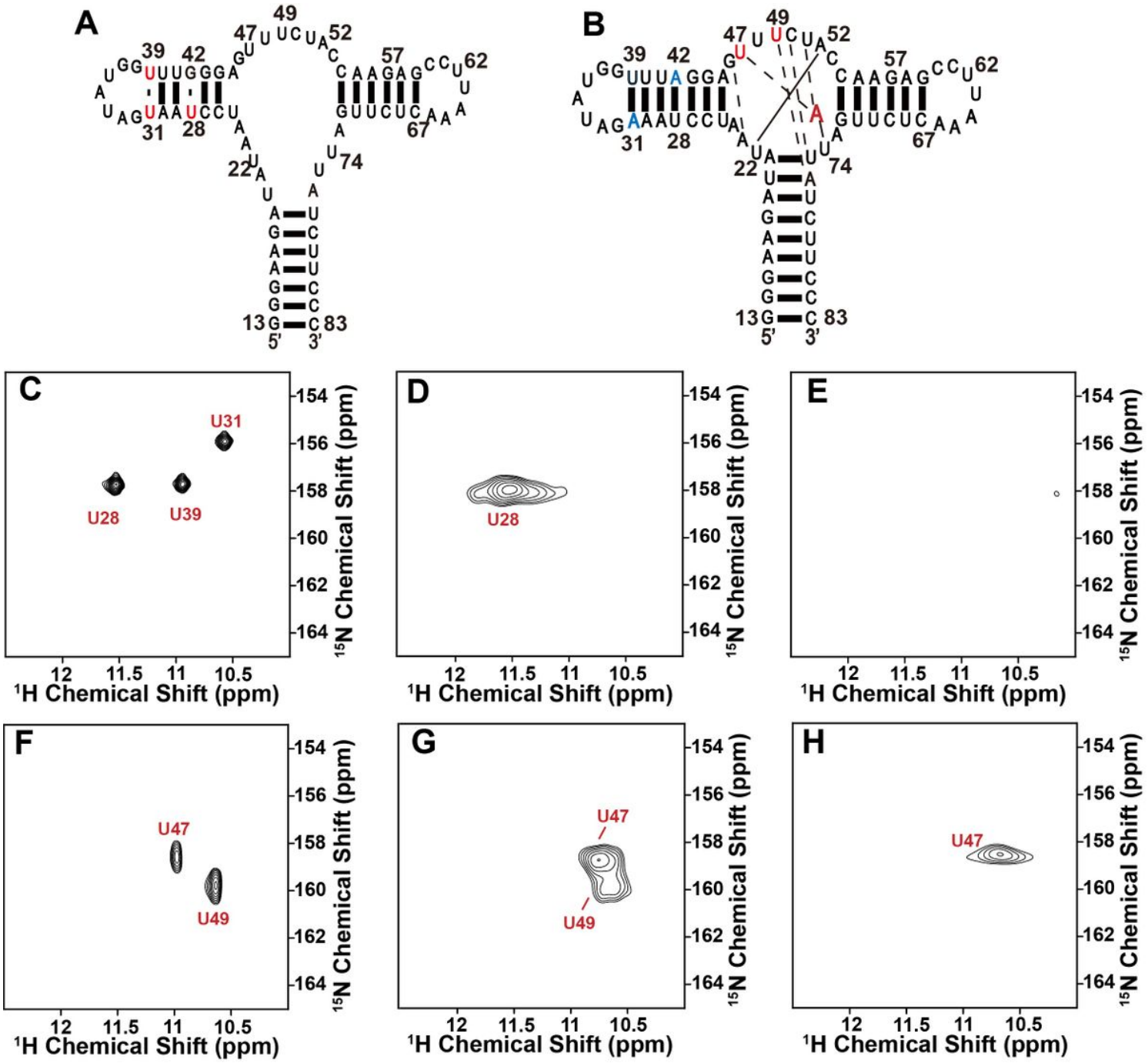

Figure 4

SSNMR and solution NMR spectra of free wild-type riboA71 and mutated riboA71-adenine complex. (A, B) Secondary structures of free wild-type riboA71 (A) and the mutated riboA71–adenine complex (B). (C) Two-dimensional (2D) 1H-15N HSQC spectrum of free wild-type riboA71 in solution. (D–E) 2D hNH (D) and 2D water–RNA exchange spectroscopy (WaterREXSY) spectra E) of free wild-type riboA71 in the solid state. (F) 2D 1H-15N HSQC spectrum of the mutated riboA71–adenine complex in solution. (G–H) 2D hNH (G) and 2D WaterREXSY spectra (H) of the mutated riboA71–adenine complex in the solid state. The spin lock-time was set at 2 ms in both 2D WaterREXSY experiments. Only the regions of uridine imino groups in non-canonical base pairs are shown.

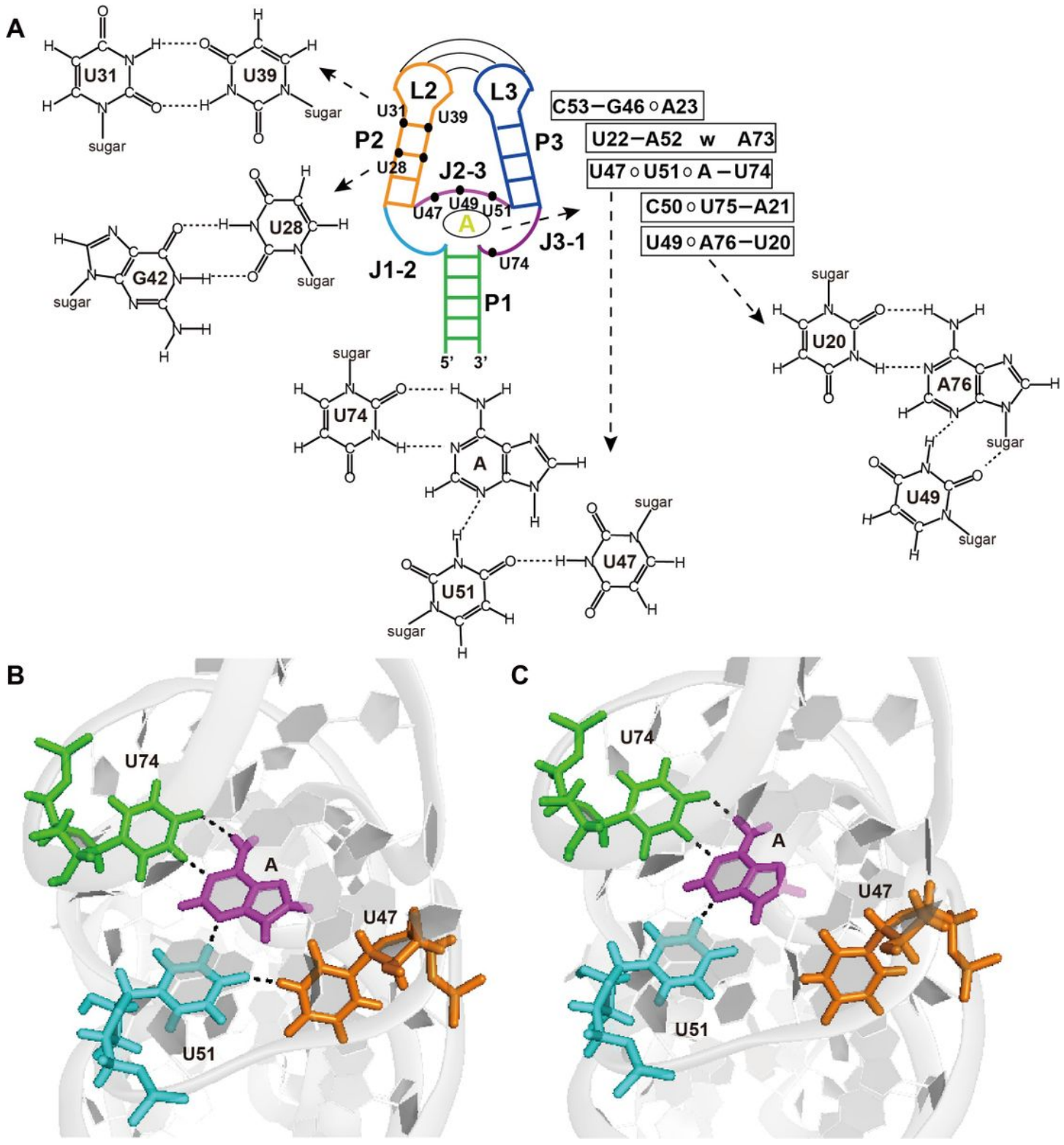

Figure 5

The topological view of riboA71-adenine complex. (A)The locations of the non-canonical base-pairs involving uridines are highlighted in the structure, e.g., U31, U39, U28 on stem P2 and U47, U49, U51 on J2-3. U31•U39, U28•G42 non-canonical base pairs are shown on the left of the model. Five-tiered arrangement of bases are shown on the right of model and (U20-A76) •U49 base triple,U47•U51•(adenine-

U74) base tetrad are also shown. (B-C) Close(B) and open(C) state of U47•U51 base pair in U47•U51•(adenine-U74) base tetrad.

Supplementary Files

This is a list of supplementary files associated with this preprint. Click to download.

- U47U49BasePairOpening.mov
- SupportingWaterREXSYfinal.pdf